Available online at www.sciencedirect.com

SciVerse ScienceDirect

Scripta Materialia 66 (2012) 562–565

Scripta MATERIALIA

www.elsevier.com/locate/scriptamat

Carbon-coated mesoporous SnO_2 nanospheres as anode material for lithium ion batteries

Fei Wang,* Xiaoping Song, Gang Yao, Mingshu Zhao,* Rui Liu, Minwei Xu and Zhanbo Sun

MOE Key Laboratory for Non-equilibrium Synthesis and Modulation of Condensed Matter, School of Science, Xi'an Jiaotong University, Xi'an 710049, People's Republic of China

Received 7 August 2011; accepted 5 January 2012
Available online 11 January 2012

In this paper mesoporous SnO_2 nanospheres with an average diameter of about 83 nm, composed of many tiny primary particles (~10 nm) and holes, are synthesized on a large scale by a simple hydrothermal route. The as-prepared mesoporous SnO_2 nanospheres were uniformly coated with carbon by a further hydrothermal treatment in glucose aqueous solution. As anode materials for lithium-ion batteries, the core–shell SnO_2/C nanocomposites exhibit a markedly improved cycling performance.

Keywords: Tin dioxide; Carbon; Nanocomposite; Lithium-ion batteries; Electrochemistry

Lithium-ion batteries (LIBs) are considered as one of the best energy storage devices for applications ranging from portable electronic devices to electric and hybrid electric vehicles. Anode materials based on graphitic carbon materials are largely used because of their excellent cycling performance and low cost. However, graphitic carbon materials have limited theoretical specific capacity (372 mAh g^{-1}). Therefore, alternative anode materials with higher specific capacities are sought nowadays [1]. Among a large number of alternative negative materials, SnO_2-based materials are attracting growing research attention due to their high theoretical specific capacity (~790 mAh g^{-1}), suitable charge/discharge voltage range, widespread availability, low toxicity and low cost. Unfortunately, large volume changes (>200%) take place upon lithium insertion/extraction within SnO_2, resulting in electrode pulverization and severe capacity fading [2]. A few strategies have been pursued to alleviate this problem, which mainly include hollow nanostructures [3–8] and nanocomposites based on an active/inactive concepts [9–16]. The interior space in hollow nanostructures can partially accommodate the large volume change. However, without a supporting matrix, metastable hollow nanostructures are inclined to break down during the lithiation/delithiation process. In comparison, nanocomposites based on the active/inactive concept should be a more effective route to improve the cycling performance of SnO_2. Carbon materials are usually used as the inactive buffer material due to their softness and good electronic conductivity, which can not only prevent the breakdown of electrode materials during Li^+ insertion and extraction but also improve the electronic conductivity.

Herein, well-designed SnO_2/C nanocomposites are prepared by two-step hydrothermal route without using any surfactants. Sodium stannate is used to prepare nearly monodisperse mesoporous SnO_2 nanospheres and glucose is used as a precursor to obtain carbon-coated SnO_2/C nanocomposites. Both the mesoporous SnO_2 nanospheres and core–shell SnO_2/C nanocomposites have been investigated as anode material for LIBs.

For the synthesis of mesoporous SnO_2 nanospheres, 5 mmol sodium stannate (Na_2SnO_3) was dissolved in 25 ml of 0.75 M glucose aqueous solution through ultrasonic dispersion. Afterward, the clear solution was transferred to 40 ml Teflon-lined stainless steel autoclaves and heated at 180 °C for 4 h. After cooling down naturally, the precipitates were harvested by centrifugation and washed thoroughly with deionized water and ethanol, respectively. The obtained samples were dried at 60 °C

* Corresponding authors. Tel.: +86 29 82663034; fax: +86 29 82667872 (F. Wang); tel.: +86 29 82663034; fax: +86 29 82667872 (M.S. Zhao); e-mail addresses: feiwang@mail.xjtu.edu.cn; zhaomshu@mail.xjtu.edu.cn

1359-6462/$ - see front matter © 2012 Acta Materialia Inc. Published by Elsevier Ltd. All rights reserved.
doi:10.1016/j.scriptamat.2012.01.003

for 4 h and the dried precipitates were heat treated in a furnace at 550 °C for 4 h in air.

The core–shell SnO_2/C nanocomposites were synthesized by dispersing as-prepared mesoporous SnO_2 nanospheres in 25 ml of 0.75 M glucose aqueous solution. The suspension was put into 40 ml Teflon-lined stainless steel autoclaves. The autoclaves were heated at 180 °C for 4 h and then naturally cooled to room temperature. The precipitates were harvested by centrifugation and washed thoroughly with deionized water and ethanol. After drying at 60 °C for 4 h, the brown powders obtained were carbonized at 550 °C for 4 h under argon atmosphere.

The morphology and structure of the products were characterized by X-ray diffraction (XRD, Bruker D8-Advance, Cu K_α, $\lambda = 0.15406$ nm), field emission scanning electron microscopy (FESEM, JEOL JSM-7100F) and transmission electron microscopy (TEM, JEOL JEM-2100).

Electrochemical properties were tested using two-electrode Swagelok cells with lithium metal as the counter and reference electrodes. The working electrodes consisted of 80 wt.% active materials, 10 wt.% conductive material (acetylene black) and 10 wt.% binder (polyvinylidene fluoride). The electrolyte was 1 M $LiPF_6$ in a mixture of 50 vol.% ethylene carbonate and 50 vol.% diethylene carbonate. Galvanostatic charge/discharge measurement was carried out by using an Arbin BT2000 battery testing system in the voltage range of 0.02–2.0 V (vs. Li/Li^+). Cyclic voltammograms (CVs) were tested on an Ametek VMC-4 electrochemical testing system at a scan rate of 0.2 mV s^{-1} between 0 and 2.0 V (vs. Li/Li^+).

Mesoporous SnO_2 nanospheres with uniform size are synthesized on a large scale based on a simple hydrothermal method followed by the heat treating in air. Figure 1 shows the XRD pattern of mesoporous SnO_2 nanospheres. All diffraction peaks can be indexed as tetragonal rutile SnO_2 (JCPDS card no. 41-1445). The relatively broad diffraction peaks indicate the small crystallite size of the sample. By using Scherrer's formula and the full width at half maximum (FWHM) data of (1 0 1) peak, the mean crystallite size can be calculated to be 7.3 nm.

The morphology and structure of as-prepared SnO_2 was characterized by SEM and TEM. SEM images (Fig. 2a, b) show that the as-prepared SnO_2 nanoparticles are spherical in shape with a narrow size distribution and

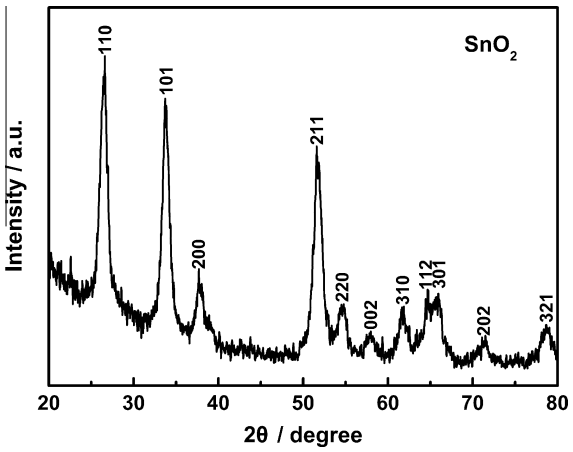

Figure 1. XRD pattern of mesoporous SnO_2 nanospheres.

nearly monodisperse feature. The diameter of the SnO_2 spheres ranges from 70 to 95 nm and the average diameter is about 83 nm (Fig. 2c). High-resolution TEM imaging (Fig. 2d) reveals that an individual SnO_2 nanosphere is comprised of many tiny primary particles and holes. The size of crystalline domains in the sphere is about 10 nm, which is consistent with the result calculated from XRD data. The corresponding selected-area electron diffraction (SAED) pattern indicates that the mesoporous nanospheres are polycrystalline and the diffraction rings can be indexed to the (1 0 1) and (1 1 0) planes of tetragonal rutile SnO_2 (Fig. 2d, inset). Usually, it is very difficult to precipitate SnO_2 nanospheres in a stannate water solution. In the present stannate water solution route, the formation of mesoporous SnO_2 nanospheres is attributed to the mildly acidic condition created by the hydrothermal treatment of glucose, which mediates the rapid precipitation of spherical SnO_2 particles. [15].

Hydrothermal treatment of the mesoporous SnO_2 nanospheres in aqueous glucose solution, yielded SnO_2/polysaccharide (carbon-rich) precursor with core–shell structure (Fig. 3a). The spherical SnO_2 particles are well embedded in the individual polysaccharide shells, and each irregular polysaccharide shell includes several SnO_2 particles. The hydrothermal treatment of glucose is an intermediate process to form carbon-rich polysaccharide. The subsequent carbonization step is essential to form absolute carbon materials. Figure 3b reveals the morphology of the core–shell SnO_2/C nanocomposites after sintering. The morphology is similar to that of the precursor, while the carbon layer thickness was reduced due to the shrinkage of polysaccharide precursor during the carbonization process.

SnO_2-based materials have been proposed as alternative anode materials with high-energy densities in LIBs. We investigated the potential use of the mesoporous SnO_2 nanospheres and carbon-coated SnO_2/C nanocomposites as LIB anode materials. Figure 4a shows the first five CV curves of mesoporous SnO_2 nanospheres at a scan rate of 0.2 mV s^{-1}. During the first cathodic scan, the peak at about 0.75 V is ascribed to the reduction of SnO_2 ($SnO_2 + 4Li^+ + 4e^- \leftrightarrow Sn + 2Li_2O$) and the broad peak extending to 0 V corresponds to the formation of different Li_xSn alloys ($Sn + xLi^+ + xe^- \leftrightarrow Li_xSn$, $0 \leqslant x \leqslant 4.4$). Two corresponding anodic peaks are observed in first anodic scan. The first peak near 0.7 V indicates the dealloying reaction of Li_xSn and the relatively weak peak at high voltage (about 1.2 V) can be ascribed to the partial reduction of Li_2O [8].

Galvanostatic charge and discharge tests were carried out between 0.02 and 2.0 V (vs. Li/Li^+) at 0.1 C for mesoporous SnO_2 nanospheres and 0.3 C for core–shell SnO_2/C nanocomposites (Fig. 4b). The mesoporous SnO_2 nanospheres have an initial discharge and charge capacity of 1846 and 827 mAh g^{-1}, respectively. The low initial coulomb efficiency (44.8%) is mainly attributed to the initial irreversible formation of Li_2O and inevitable formation of solid electrolyte interface (SEI layer). The discharge capacity in the second cycle can reach 1000 mAh g^{-1}. Such a high lithium storage capacity is associated with the partial reversible oxidation/reduction of Li_2O, which is consistent with the 1.0 V peak in the cathodic scan and the 1.2 V peak in the anodic scans in

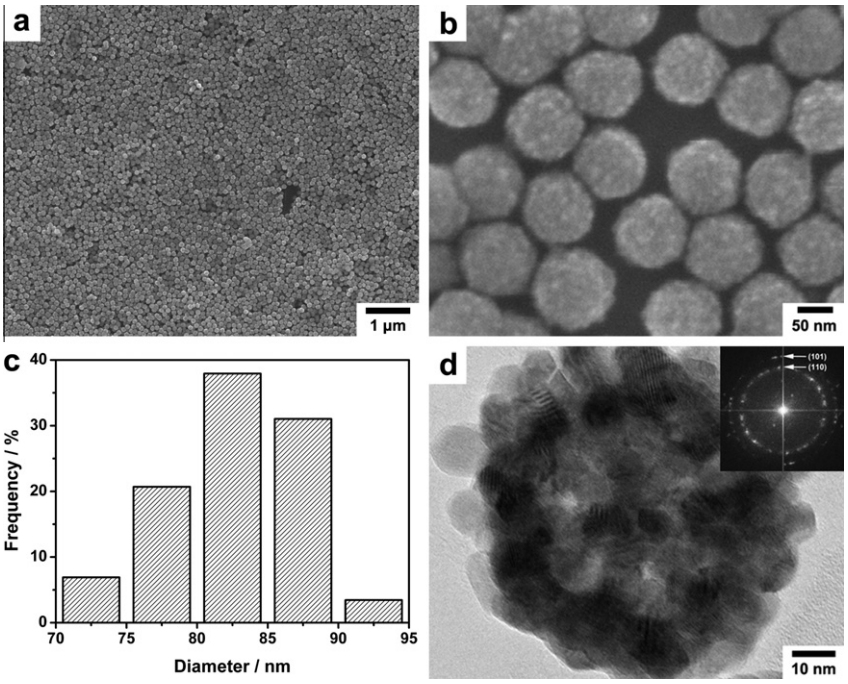

Figure 2. (a, b) SEM images of mesoporous SnO_2 nanospheres; (c) the size distribution of mesoporous SnO_2 nanospheres; (d) HRTEM image of an individual mesoporous SnO_2 nanosphere. The inset in (d) shows the SAED pattern of an individual mesoporous SnO_2 nanosphere.

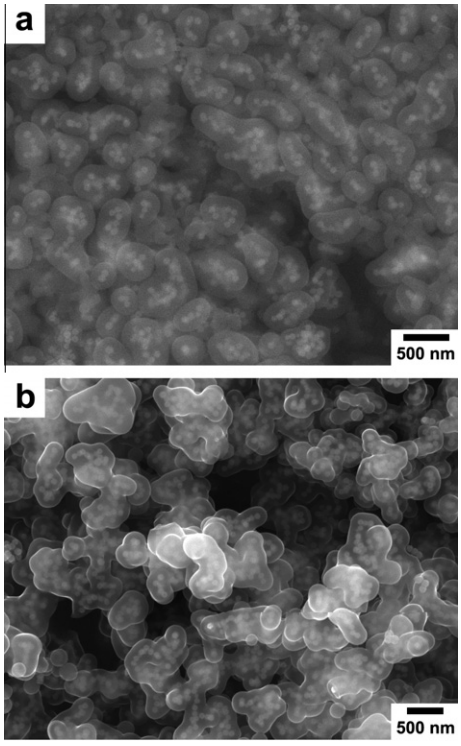

Figure 3. (a) SEM image of as-prepared core–shell SnO_2/polysaccharide precursor and (b) SEM image of core–shell SnO_2/C nanocomposites.

CV tests. From the second cycle, the capacity rapidly declines to about 200 mAh g^{-1} over 50 cycles. The poor cycling performance indicates the collapse of mesoporous SnO_2 nanostructure for the lack of a supporting matrix. In comparison, the core–shell SnO_2/C nanocomposites exhibit superior cycling performance even at a relatively

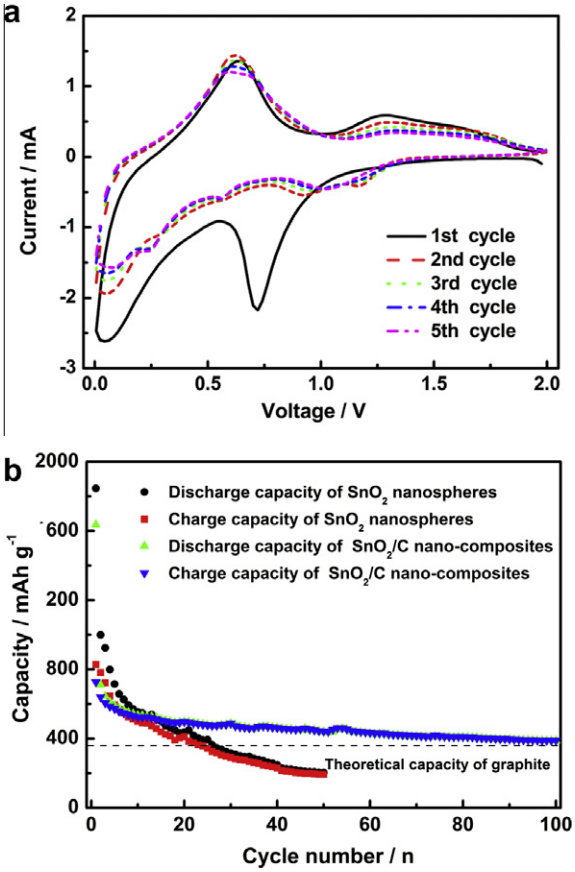

Figure 4. (a) CV curves of mesoporous SnO_2 nanospheres; (b) cycling performance of mesoporous SnO_2 nanospheres at 0.1 C and core–shell SnO_2/C nanocomposites at 0.3 C.

high current density (0.3 C). The discharge capacity can be maintained at about 390 mAh g^{-1} after 100 cycles, which is higher than the theoretical value of commercial graphite (372 mAh g^{-1}). Thus, the carbon shell serves as a physical buffer which can effectively prevent the structural breakdown of mesoporous SnO_2 nanospheres.

In summary, mesoporous SnO_2 nanospheres have small particle sizes and hollow interiors, and exhibit rapid capacity fading with charge/discharge cycling. Coating the mesoporous SnO_2 nanospheres uniformly with carbon resulted in a markedly improved cycling performance of the core–shell SnO_2/C nanocomposites. Thus, nanocomposites based on the active/inactive concept are a more effective route to improve the cycling performance of SnO_2.

This work was supported by National Natural Science Foundation of China (51002117), Specialized Research Fund for the Doctoral Program of Higher Education of China (20100201120049) and Fundamental Research Funds for the Central Universities (0109-08141012, 08143017, 08143029).

[1] M.R. Palacín, Chem. Soc. Rev. 38 (2009) 2565.
[2] I.A. Courtney, J.R. Dahn, J. Electrochem. Soc. 144 (1997) 2045.
[3] Z.Y. Wang, D.Y. Luan, F.Y.C. Boey, X.W. Lou, J. Am. Chem. Soc. 133 (2011) 4738.
[4] J.F. Ye, H.J. Zhang, R. Yang, X.G. Li, L.M. Qi, Small 6 (2010) 296.
[5] M.W. Xu, M.S. Zhao, F. Wang, W. Guan, S. Yang, X.P. Song, Mater. Lett. 64 (2010) 921.
[6] D. Deng, J.Y. Lee, Chem. Mater. 20 (2008) 1841.
[7] H.X. Yang, J.F. Qian, Z.X. Chen, X.P. Ai, Y.L. Cao, J. Phys. Chem. C 111 (2007) 14067.
[8] S.J. Han, B.C. Jang, T. Kim, S.M. Oh, T. Hyeon, Adv. Funct. Mater. 15 (2005) 1845.
[9] X.Y. Wang, X.F. Zhou, K. Yao, J.G. Zhang, Z.P. Liu, Carbon 49 (2011) 133.
[10] P.C. Lian, X.F. Zhu, S.Z. Liang, Z. Li, W.S. Yang, H.H. Wang, Electrochim. Acta 56 (2011) 4532.
[11] F. Wang, G. Yao, M.W. Xu, M.S. Zhao, Z.B. Sun, X.P. Song, J. Alloys Compd. 509 (2011) 5969.
[12] J. Liu, W. Li, A. Manthiram, Chem. Commun. 46 (2010) 1437.
[13] G.D. Du, C. Zhong, P. Zhang, Z.P. Guo, Z.X. Chen, H.K. Liu, Electrochim. Acta 55 (2010) 2582.
[14] S.J. Ding, D.Y. Luan, F.Y.C. Boey, J.S. Chen, X.W. Lou, Chem. Commun. 47 (2011) 7155.
[15] X.W. Lou, J.S. Chen, P. Chen, L.A. Archer, Chem. Mater. 21 (2009) 2868.
[16] C.Q. Feng, L. Li, Z.P. Guo, H. Li, J. Alloys Compd. 504 (2010) 457.